JACS
JOURNAL OF THE AMERICAN CHEMICAL SOCIETY
Article
pubs.acs.org/JACS

How do Enzymes Utilize Reactive OH Radicals? Lessons from Nonheme HppE and Fenton Systems

Binju Wang,*[,†] Jiarui Lu,[‡] Kshatresh Dutta Dubey,[†] Geng Dong,[‡] Wenzhen Lai,*[,‡] and Sason Shaik*[,†]

[†]Institute of Chemistry and The Lise Meitner-Minerva Center for Computational Quantum Chemistry, The Hebrew University of Jerusalem, 91904 Jerusalem, Israel

[‡]Department of Chemistry, Renmin University of China, Beijing 100872, China

Supporting Information

ABSTRACT: The iron(IV)−oxo (ferryl) intermediate has been amply established as the principal oxidant in nonheme enzymes and the key player in C−H bond activations and functionalizations. In contrast to this status, our present QM/MM calculations of the mechanism of fosfomycin biosynthesis (a broad range antibiotic) by the nonheme HppE enzyme rule out the iron(IV)−oxo as the reactive species in the hydrogen abstraction (H-abstraction) step of the pro-*R* hydrogen from the (*S*)-2-hydroxypropylphosphonic substrate. Moreover, the study reveals that the ferryl species is bypassed in HppE, while the actual oxidant is an HO• radical hydrogen-bonded to a ferric-hydroxo complex, resulting via the homolytic dissociation of the hydrogen peroxide complex, Fe(II)−H_2O_2. The computed energy barrier of this pathway is 12.0 kcal/mol, in fair agreement with the experimental datum of 9.8 kcal/mol. An alternative mechanism involves the iron-complexed hydroxyl radical (Fe^{III}−(HO•)) that is obtained by protonation of the iron(IV)−oxo group via the O−H group of the substrate. The barrier for this pathway, 23.0 kcal/mol, is higher than the one in the first mechanism. In both mechanisms, the HO• radical is highly selective; its H-abstraction leading to the final *cis*-fosfomycin product. It appears that HppE is prone to usage of HO• radicals for C−H bond activation, because the ferryl oxidant requires a specific H-abstraction trajectory (∠FeOH ∼ 180°) that cannot be met for intramolecular H-abstraction. Thus, this work broadens the landscape of nonheme iron enzymes and makes a connection to Fenton chemistry, with implications on new potential biocatalysts that may harness hydroxyl radicals for C−H bond functionalizations.

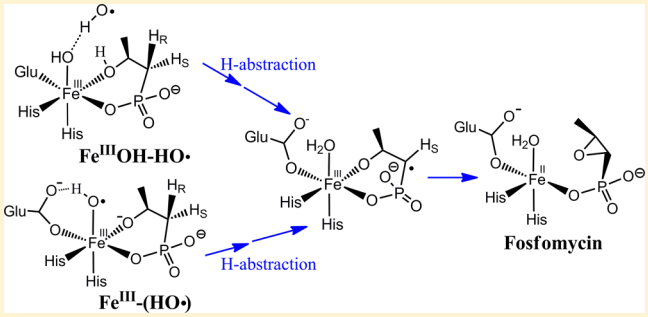

1. INTRODUCTION

Nature has evolved a toolbox of various oxidants to accomplish many challenging reactions in metalloenzymes. One of the key oxidants in metalloenzymes is the high-valent iron(IV)−oxo intermediate,[1−3] which performs a variety of oxidative reactions in C−H bond activations and functionalizations.[4−6] In many of these nonheme enzymes, the resting state involves an Fe(II) core. As such, we must recall that Fe(II)-dependent oxidations in the presence of H_2O_2 may generate via the Fenton reaction another powerful oxidant, the hydroxyl radical HO•.[7] This species poses a serious threat to aerobic organisms, such that naturally occurring scavenger enzymes, like catalase and superoxide dismutase, have evolved to neutralize the hydroxyl radical. Indeed, the presence of HO• species as a "competent oxidant" in naturally occurring enzymes is generally viewed with much skepticism, because HO• is such a highly unselective species that may damage the surrounding protein and destroy the enzymatic activity.[8] Nevertheless, we report herein a case of an enzymatic oxidation by a nonheme enzyme that harnesses the HO• radical to perform a most energy-demanding step, namely, C−H activation. This is the (*S*)-2-hydroxypropylphosphonic (*S*-HPP) acid epoxidase (HppE) enzyme that catalyzes the oxidative epoxidation reaction of *S*-HPP, as the ultimate step in the biosynthesis of the broad range antibiotic fosfomycin (fos).[9−14]

HppE was initially characterized as an Fe(II)-dependent oxidant, which was thought to use O_2 and external reductants to accomplish the biosynthesis of fosfomycin.[9−14] However, a more recent study demonstrated unequivocally that HppE is an H_2O_2-dependent peroxidase, rather than O_2-dependent oxidase.[13] Scheme 1 depicts the proposed mechanism of HppE for the biosynthesis of fosfomycin.[13] It is thought that the reaction of the Fe^{II} cofactor with H_2O_2 leads to the formation of the ferryl Fe^{IV}=O species, which proceeds to abstract an H atom from *S*-HPP to form a C1-based radical intermediate. The subsequent electron transfer from the C1-radical to Fe^{III} leads to a carbocation intermediate,[13,15] which is thought to undergo ring-closure to the final fosfomycin product, which has a *cis*-epoxide ring.

While the Fe^{IV}=O species has been trapped and characterized in a number of nonheme enzymes and synthetic

Received: April 6, 2016
Published: June 16, 2016

ACS Publications © 2016 American Chemical Society

DOI: 10.1021/jacs.6b03555
J. Am. Chem. Soc. 2016, 138, 8489−8496

Scheme 1. Proposed Mechanism of HppE for the Fosfomycin Biosynthesis

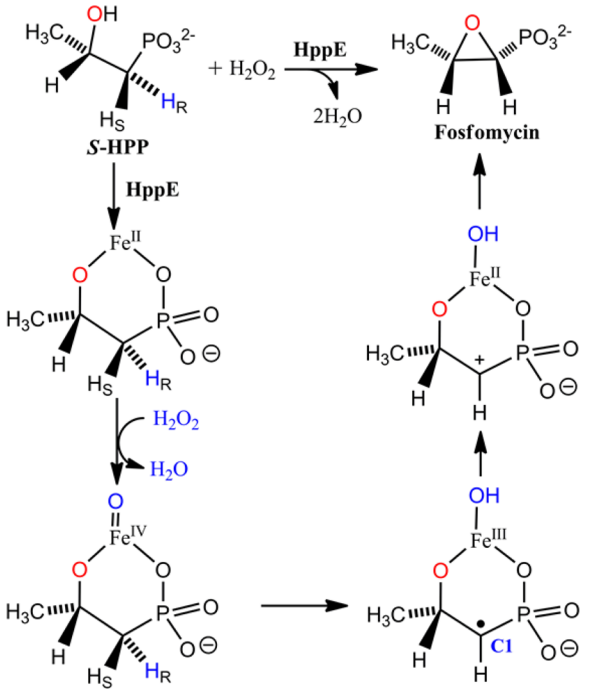

complexes[1,2,6,16,17] and was proven to be a highly competent oxidant, there is no direct experimental evidence of the involvement of Fe^{IV}=O in HppE. Nevertheless, a recent quantum mechanical (QM) study using model calculations lends some support to the formation of Fe^{IV}=O species.[18] This theoretical study proposed that the actual oxidant that abstracts the H_R hydrogen from the substrate is in fact the oxyl radical, Fe^{III}–O•, which is an excited state of the ferryl Fe^{IV}=O species.[18] At the same time, however, the QM calculations predicted that the ring-closure transpires with a preferred formation of *trans*-epoxide rather than the experimentally observed *cis*-epoxide (fos), as shown in Scheme 1. This proposal remains therefore inconclusive, and the reactivity scenario requires reexamination.

Indeed, as we mentioned at the outset, the reaction of Fe(II) with H_2O_2 in HppE is a typical Fenton reaction, which may give rise to the highly reactive HO• species. Therefore, one must establish the role if any of this species along with the oxyl Fe^{III}–O• and the ferryl Fe^{IV}=O, the latter being the key oxidant in nonheme enzymes. To these ends, we carried out quantum mechanical/molecular mechanical (QM/MM) calculations, which can yield reliable atomistic information on structures and mechanisms within the native environment of the protein.[19−22] As shall be demonstrated, our QM/MM calculations rule out the Fe^{IV}–oxo and its Fe^{III}–O• electromer as the C–H activators in HppE. At the same time, the QM/MM calculations show that HppE is prone to usage of a coordinated HO• radical as the only oxidant capable of facile C–H activation in HppE, leading eventually to the correct stereochemistry of the epoxide product (Scheme 1). Thus, our study shows how an enzyme generates a highly reactive HO• radical and tames it for usage in selective C–H activations. The implications on Fenton chemistry are also discussed.

2. COMPUTATIONAL METHODS

2.1. Setup of the QM/MM System. The initial structure of the enzyme-substrate complex was prepared on the basis of the X-ray structure of the HppE enzyme (PDB code: 1ZZ8, with a resolution of 2.3 Å).[12] The crystal structure of 1ZZ8 contains two identical subunits, A and B. In the model setup, the whole chain A was kept. For the chain B, we kept residues 6−73 that extend into chain A, and the residue 6 was treated as N terminal, while the residue 73 was treated as C terminal, while all the rest of the residues were omitted. The neighboring crystal water to Fe in the active site of chain A is replaced by H_2O_2.

We assigned the protonation states of titratable residues (His, Glu, Asp) on the basis of pK_a values using PROPKA[23] in combination with careful visual inspection of local H-bonded networks. The histidine residues His61 and His152 were protonated at the ϵ position, and the histidine residues His138 and His180 were protonated at the δ position, while all the rest of the histidine residues were doubly protonated. All glutamic acid and aspartic acid residues were deprotonated. The resulting system had a net charge of −13, which was neutralized by protonating titratable residues on the surface of the protein.

After adding all hydrogens, the positions of the hydrogen (H) atoms were optimized with 200 steps of steepest descent and 200 steps of the adapted basis Newton−Raphson method using the CHARMM27 force fields implemented in the CHARMM program.[24] The resulting protein was solvated with a 16 Å layer of TIP3P water. Then, to attain equilibrium of the inner solvent layer, we followed four steps: (1) optimization of the inner solvent layer for 1000 steps of steepest descent and 1000 steps of the adapted basis Newton−Raphson method; (2) heating slowly the protein from 0 to 300 K for 15 ps with a 1 fs time step; (3) equilibrating the solvent layer for 15 ps at 300 K with a 1 fs time step; and (4) resolvation of the protein to fill up the interspace of the solvent layer. These four steps were repeated four times until no more than 50 water molecules were added into the interspace of the solvent layer. After these procedures, a productive molecular dynamics (MD) run was performed. First, we employed a 10 ns MD in which the coordinates of the entire Fe(II)−H_2O_2 unit and the metal-ligating residues as well as the outer 8 Å of the solvent layer were kept frozen. Subsequently, we ran the MD for 20 ns while now allowing the H_2O_2 unit to fully relax. From these MD trajectories we selected two snapshots of the Fe(II)−H_2O_2 complex: Snap-1 represents the MD with frozen Fe(II)−H_2O_2 unit and early MD trajectory in the relaxed MD, while Snap-2 is taken from the converged and majority part of the relaxed MD, at about 10 ns of the trajectory (see Figure S1). These two snapshots, Snap-1 and -2, are used in the QM/MM calculations. As will be seen, the H_2O_2 molecule, which is a weak binder to Fe(II), is flexible and subject to many H-bonds, so the relaxed MD is the method of choice.

2.2. QM/MM Methodology. All QM/MM calculations were performed using ChemShell,[25] combining Turbomole[26] for the QM region and DL_POLY[27] for the MM region. The CHARMM27 force field was employed throughout this study for the MM region.[24] The electronic embedding scheme[28] was used to account for the polarizing effect of the enzyme environment on the QM region. Hydrogen link atoms with the charge-shift model[25] were applied to treat the QM/MM boundary. During QM/MM geometry optimizations, the QM region was studied with the hybrid UB3LYP[29] density functional with two levels of theory. For geometry optimization and frequency calculations, all-electron the basis of Def2-SVP (labeled as B1) was used. The energies were further corrected with the larger basis set Def2-TZVP (labeled as B2). All the transition states (TSs) were located by relaxed potential energy surface (PES) scans followed by full TS optimizations using the P-RFO optimizer implemented in the HDLC code.[30] The empirical dispersion energy correction was also added by using the DFT-D3 program.[31]

The QM region consists of the first-coordination sphere residues of Fe in the active site, which are two histidines (His138 and His180), one glutamic acid (Glu142), substrate *S*-HPP, and H_2O_2. Lys23 residue in chain B is also included in the QM region, as it is positioned

DOI: 10.1021/jacs.6b03555
J. Am. Chem. Soc. 2016, 138, 8489−8496

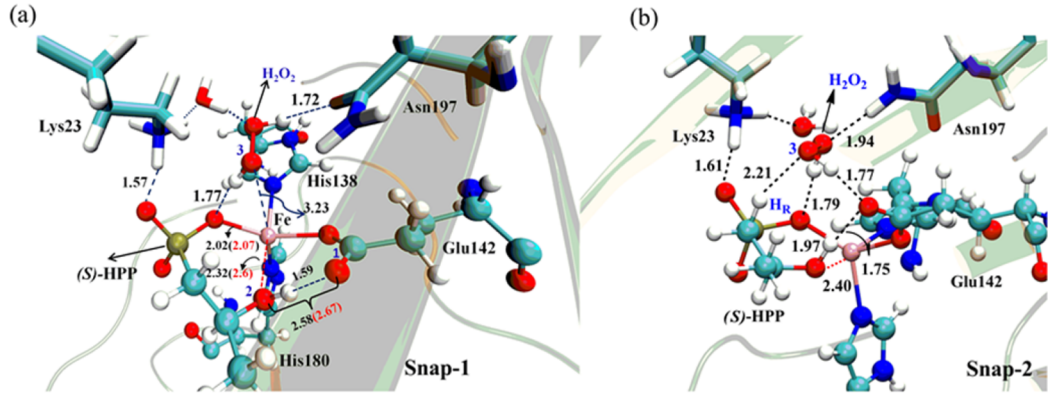

Figure 1. QM/MM optimized reactant complexes taken from the two snapshots Snap-1 in (a), while Snap-2 in (b) of the equilibrium MD trajectory of the Fe^{II}–H_2O_2 system. The key QM/MM distances (in Å) in the Figure are given in black, while the values from the crystal structure (PDB: 1ZZ8; see Figure 1a) are shown in red, in parentheses. Note the match of the computed distances to experiment.

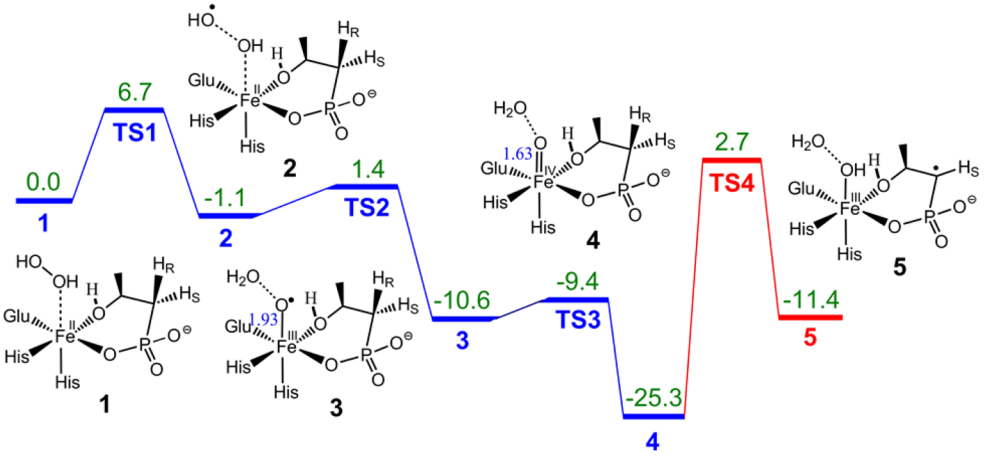

Figure 2. QM/MM (UB3LYP/B2) relative energies (kcal/mol) for Fe^{III}–$O^{\bullet}$/Fe^{IV}=O (**3**/**4**) formation from the Fe^{II}–H_2O_2 complex (**1** from Snap-1) and the H-abstraction by Fe^{IV}=O to yield **5**. The ZPE and dispersion corrections are included in the relative energies. The Lys23 and Asn197 maintain H-bonding with H_2O_2, but omitted in the structures to avoid crowding the figure. The pathway not taken from **4** to **5** is drawn in a red line.

in the active site. The overall charge of the QM model is zero. The calculated triplet and singlet states are 26.1 and 47.0 kcal/mol higher than the quintet state in Fe(II)–H_2O_2 complex at B3LYP/B2, respectively. For Fe(IV)=O, the calculated triplet and singlet states are 13.8 and 22.8 kcal/mol above the quintet state. In addition, the calculated H-abstraction barrier from the triplet state is ~28 kcal/mol (Figure S2), so that the corresponding overall barrier for H-abstraction is over 40 kcal/mol relative to quintet Fe(IV)=O species. Since the singlet is even higher lying, we did not further investigate its reactivity. For the Fe(III)–$O^{\bullet}$ species, the calculated triplet and singlet states are 16.3 and 22.7 kcal/mol higher than the quintet state. As seen later, the H-abstraction by Fe(III)–$O^{\bullet}$ species in the quintet state has a barrier of 10.4 kcal/mol (Figure 3), so that the triplet and singlet states of Fe(III)–$O^{\bullet}$ will not cross the quintet energy surface. Therefore, all the calculations will focus on the quintet spin state, since it is both the ground state and the only reactive state for the reactions of interest in this work. Our QM/MM calculations are based on a well-tested procedure,[32−35] which has proven reliable for iron-based metalloenzymes.

3. RESULTS AND DISCUSSION

3.1. The QM/MM Optimized Structures of $Fe^{II}(H_2O_2)$ Reactant Complexes. Figure 1a,b show the QM/MM optimized Fe(II)–H_2O_2 complexes from the two snapshots. Thus, as seen in Figure 1a for Snap-1, the active site of HppE contains an iron center ligated by two histidines (His138 and His180) and one glutamate (Glu142). The substrate coordinates to Fe^{II} via its phosphonic oxygen bound *trans* to Glu142, while the substrate's O2 atom remains uncoordinated to Fe^{II}. The crystal structure of 1ZZ8 shows that the hydroxyl oxygen (O2) has a very short distance with the O1 of Glu142 (2.67 Å as shown in Figure 1a),[12] thus suggesting a strong H-bond could exist between them. The Fe–O2 distance in the crystal structure is 2.60 Å, suggesting the hydroxyl oxygen of *S*-HPP is not coordinated to Fe^{II}, or only very weakly so. Based on this analysis of the crystal structure, the substrate is protonated at O2, i.e. O2–H. The QM/MM-optimized structure in Figure 1a shows a good match with the crystal structure and thus supports our assignment that the substrate is protonated at hydroxyl oxygen (O2). These features are common also to Snap-2 in Figure 1b. In both cases the hydrogen peroxide is held by a mesh of H-bonds, which make it persistent in the active site. The main differences between the two snapshots are the H-bonding networks as well as the H_2O_2 orientation in the active site. In Snap-1, H_2O_2 is far away from the target H_R of (*S*)-HPP, while in Snap-2, the distal O3 of H_2O_2 has a short distance to H_R of (*S*)-HPP (O3···H_R distance is 2.21 Å in Figure 1b).

3.2. Fe^{III}–$O^{\bullet}$/Fe^{IV}=O Species Formation and C–H Activation by Fe^{IV}=O Species. Initially we started the QM/MM from Snap-1 in Figure 1a, with an aim of resolving the status of Fe^{IV}=O and Fe^{III}–$O^{\bullet}$ as potential oxidants of

DOI: 10.1021/jacs.6b03555
J. Am. Chem. Soc. 2016, 138, 8489−8496

HppE. Figure 2 shows the QM/MM reaction-energy profile starting from the $Fe^{II}-H_2O_2$ reactant complex, based on the experimentally proposed mechanism in Scheme 1. The $Fe^{II}-H_2O_2$ complex has a quintet ground state with four unpaired electrons in the d-orbitals of iron (see Figure S3). Starting from $Fe^{II}-H_2O_2$ (**1**), the initial homolytic O−O bond cleavage via **TS1** leads to a $Fe^{III}-OH$ species along with an $HO^{\bullet}$ radical (**2**). The so-generated **2** maintains an antiferromagnetic coupling of high-spin Fe^{III} with the $HO^{\bullet}$ radical (Figure S4), in which the O atom of the $HO^{\bullet}$ radical has a negative spin density of −0.85.

The so-formed $HO^{\bullet}$ in **2** is oriented by H-bonding interactions with Lys23 and Asn197 residues (Figure S5), so that it is constrained to abstract the H from $Fe^{IV}OH$ via **TS2**, thereby generating the oxyl $Fe^{III}-O^{\bullet}$ species (**3**), which is seen to possess a long Fe−O distance of 1.93 Å. We also considered the H-abstraction from Lys23 by $HO^{\bullet}$, but the QM/MM calculations show $HO^{\bullet}$ is unable to abstract H from Lys23 (Figure S6). The oxyl species **3** can easily convert to the corresponding $Fe^{IV}{=}O$ ferryl species (**4**) via **TS3** by Fe−O bond shrinkage. Starting from **4**, we investigated the pro-*R* H-abstraction from the substrate by $Fe^{IV}{=}O$ through **TS4**, which leads to **5** with a low-spin Fe(III). However, as seen in the red energy profile in Figure 2, the QM/MM energy barrier is 28.0 kcal/mol. As such, the $Fe^{IV}{=}O$ species is not really reactive toward $C-H_R$ activation in HppE. This may seem unusual, in view of the widely accepted potency of nonheme $Fe^{IV}{=}O$ species as H-abstractors. However, we should recognize that the ideal Fe−O—H angle in H-abstraction TS should be close to 180°,[36] whereas the intramolecular H-abstraction in **TS4** is constrained to ∼103° thus leading to a high barrier.[37] What is required in H-abstraction is an oxidant that does not have a rigid geometric requirement. The following sections explore two such candidates.

3.3. Reactivity of $Fe^{III}-O^{\bullet}$ toward C−H Activation and $Fe^{III}-(HO^{\bullet})$ Formation. The first alternative candidate to explore is the $Fe^{III}-O^{\bullet}$ species, **3**, which was suggested by the QM-study to be the active species.[18] Figure 3 displays the two competing reaction pathways available to $Fe^{III}-O^{\bullet}$. One pathway, to the left, involves pro-*R* H-abstraction via **TS5**, leading to **6** with a high-spin Fe(III) (see Figure S7). This step possesses a barrier of 10.4 kcal/mol relative to **3**. The alternative pathway available to **3** is the abstraction of the substrate's hydroxyl proton (H1 linked to O2) and relaying it to O3 of the oxyl, eventually resulting in **8**. This is a two-step process and assisted by the Glu142 residue; initially, the proton is transferred from O2 to O1 of Glu142 to form **7** via **TS6**, with a barrier of 7.9 kcal/mol (**3** → **TS6**). The subsequent proton transfer from O1 to O3 via **TS7** is barrier-free, leading to the $Fe^{III}-(HO^{\bullet})$ species **8**, wherein the $HO^{\bullet}$ radical is loosely bound. The formation of **8** from $Fe^{III}-O^{\bullet}$ species (blue energy profile) is seen to be more favorable than the pro-*R* H-abstraction by $Fe^{III}-O^{\bullet}$ species (red energy profile).

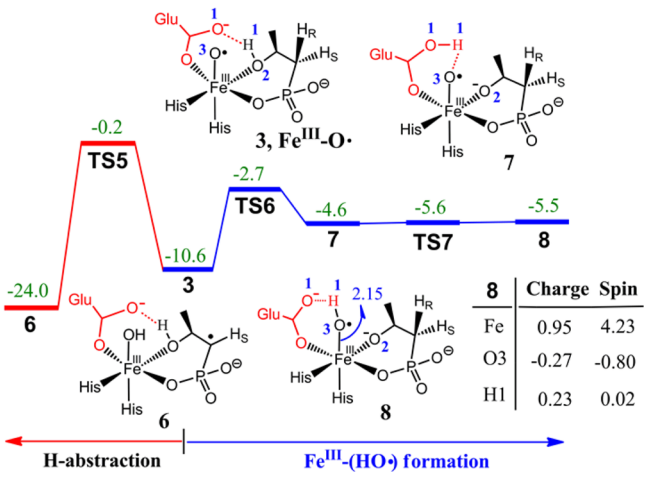

Figure 3. QM/MM (UB3LYP/B2) relative energies (kcal/mol) for the competition of H-abstraction and $Fe^{III}-(HO^{\bullet})$ formation starting from the $Fe^{III}-O^{\bullet}$ species, **3**. The red profile, leading to **6**, is the path not taken. The lower-energy path is shown in the blue profile and leading to **8**. ZPE and dispersion corrections are included in the relative energies. The Mulliken charge and spin densities of $Fe^{III}-(HO^{\bullet})$ species are also shown alongside.

The so-formed $Fe^{III}-(HO^{\bullet})$ species (**8**) is quite unusual. First, its Fe···OH distance is very long with a value of 2.15 Å, suggesting that there is not much covalent bonding between Fe and OH moiety. Second, **8** has six unpaired electrons and involves an antiferromagnetic coupling of high-spin Fe^{III} with the $HO^{\bullet}$ radical (Figure S8). The population analysis shows O3 of the HO moiety has a large negative spin density (−0.80), while its group charge is close to zero (Figure 3). These features indicate that the HO moiety is mostly an $HO^{\bullet}$ radical that is weakly bound to Fe^{III}. The geometric features of **8** indicate a strong bonding of the deprotonated O2 ligand with Fe^{III}. This strong $Fe^{III}-O2$ bonding increases in turn the antibonding character of the d-orbitals of the iron and prevents the O(3)H moiety to form by itself a strong bond to iron (see Figure S8). Moreover, the high-spin ferric ion in $Fe^{III}-(HO^{\bullet})$ is stabilized by the exchange enrichment[36,38] (see Figure S8). These factors, taken together, stabilize the $Fe^{III}-(HO^{\bullet})$ species. For **8**, the putative sister-state with ferromagnetic coupling between Fe^{III} (S = 3/2) and hydroxyl radical (S = 1/2) could not be located, as it was variationally unstable because of its higher energy. In the following section, we proceed to consider the reactivity of this loosely bound hydroxyl radical species **8**.

3.4. Reactivity of $Fe^{III}-(HO^{\bullet})$ toward C−H Activation and Fosfomycin Formation. Figure 4a shows the QM/MM calculated energy profile for the C−H activation and fosfomycin formation starting from $Fe^{III}-(HO^{\bullet})$, **8**. It is seen that the pro-*R* H-abstraction from the substrate by $Fe^{III}-(HO^{\bullet})$ species via **TS8** requires now a tiny barrier of 3.2 kcal/mol relative to **8**, leading to $Fe^{III}-H_2O$ and a C1-based substrate radical complex, **9**, which involves an antiferromagnetic coupling of high-spin Fe^{III} with the C1 radical center (the state with ferromagnetic coupling between Fe^{III} and hydroxyl is 14.4 kcal/mol higher than **9**.) The reactivity of $Fe^{III}-(HO^{\bullet})$ species is remarkably higher than that of $Fe^{IV}{=}O$ in C−H activation (recall, the latter has a barrier of 28.0 kcal/mol for the same H-abstraction, Figure 2). In **9**, the C1 radical site is situated above the plane formed by O4−P−C1−C2 (Figure 4b). The C1−O2 coupling in **9** via **TS9** yields the *trans*-fosfomycin (**10**, *trans*-fos). By contrast, in the alternative pathway, **9** undergoes a facile conformation change, yielding **11** via **TS10**, in which the C1 radical site is now below the plane formed by O4−P−C1−C2 (see Figure 4b). The following C1−O2 coupling via **TS11** yields the *cis*-fosfomycin (**12**, cis-fos). It is seen from Figure 4a that **TS11** is 3.4 kcal/mol lower in energy than **TS9**, indicating that *cis*-fos is indeed the preferred product, in good agreement with the experiments.[13] It should be noted we did not locate a carbocation intermediate that might have arisen by electron transfer from the C1-radical to Fe^{III}.

DOI: 10.1021/jacs.6b03555
J. Am. Chem. Soc. 2016, 138, 8489−8496

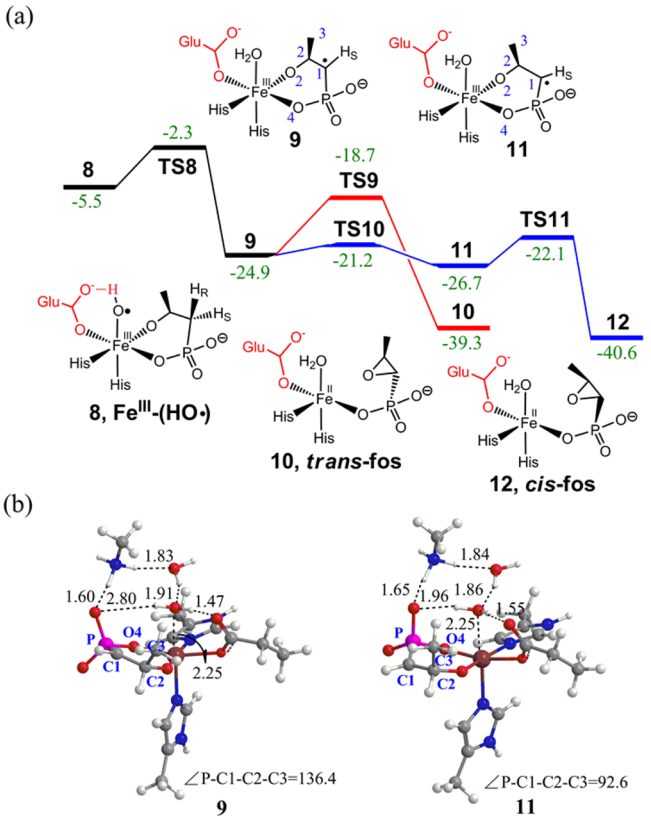

Figure 4. (a) QM/MM (UB3LYP/B2) relative energies (kcal/mol) for reactivity of Fe^{III}–(HO•) species toward C–H activation and fosfomycin formation. ZPE and dispersion corrections are included in the relative energies. The red profile to the *trans* product **10** is the path not taken, while the blue profile leading to **12** is the productive path that generates the observed *cis*-fosfomycin. (b) QM/MM (UB3LYP/B1) optimized structures of **9** and **11**; the distances are given in angstroms and the angles in degrees.

3.5. The Overall Mechanism Nascent From Snap-1.

Figure 5 collates the entire mechanistic scheme based on the QM/MM optimized structure of $Fe^{II}(H_2O_2)$ starting from Snap-1 (Figure 1a). It is seen that while Fe^{III}–(HO•) (**8**) is a truly potent oxidant in a single turnover of the enzyme, in a working enzyme with more than a single turnover, the rate-determining intermediate is the Fe^{IV}–oxo intermediate **4**, while the rate-determining TS is **TS8**, such that the overall barrier of the reaction will be 23.0 kcal/mol, and hence the catalytic cycle will be quite sluggish. This is in discord with experiment,[13] which shows a very fast cycle with k_{cat} that translates to a barrier of 9.8 kcal/mol. Thus, while Fe^{III}–(HO•) (**8**) prevails over the ferryl species in HppE, still the latter is needed to make the cycle go on. Therefore, there must be a lower energy mechanism.

3.6. Fenton-Like C–H Activation by the $Fe^{II}(H_2O_2)$ Complex (from Snap-2).

To explore a potential new mechanism, we restarted the QM/MM investigation from Snap-2 (Figure 1b). The new mechanism is displayed in Figure 6 starting from $Fe^{II}(H_2O_2)$, labeled as **1′**. The O–O bond homolysis of the latter leads to Fe^{III}–OH species that coordinates the HO• radical (**2′**). This **2′** species is analogous to **2** in Figures 2, but the HO• radical points now inward and is held by a H-bond to the oxygen substituent of the Fe^{III}–OH species. In turn, **2′** can undergo two competing H-abstraction transformations. Abstracting the H from the Fe^{III}–OH of **2′** generates the Fe^{IV}–oxo intermediate **4′**, with a barrier of 6.4 kcal/mol (red energy profile), while by H-abstraction from H_R of C1, with hardly any barrier, it generates **3′** which follows to **5′** by proton abstraction from O2–H assisted by Glu142 through **TS4′** (Figure S10). In turn, **5′** can either transform to the *trans*-fos product with a barrier of 20.3 kcal/mol (see red profile) or alternatively undergo a facile conformational change to **7′** (for the conformation change, see SI, page S8 or Figure S10) and then proceed to the final *cis*-fos product of **8′** via **TS6′**, with a barrier of 12.0 kcal/mol. The final *cis*-fos formation process is also the rate-determining step in the entire transformation. The predicted barrier of 12 kcal/mol is quite close to the experimentally derived barrier of 9.8 kcal/mol,[13] and therefore this mechanism is preferable to the one in Figure 5. Thus, once again, we find out that HppE resorts to a HO• radical (Fe^{III}(H)O···HO•, **2′**) to carry out the difficult H-abstraction of the pro-*R* hydrogen from C1.

3.7. Comparison of the Reactivity and Selectivity of Fe^{IV}=O, Fe^{III}–O•, Fe^{III}–(HO•), and Fe^{III}–OH(HO•) Species in C–H Activation in HppE.

Figure 7 ranks the oxidative capabilities of the H-abstractors in this study, by using the corresponding H-abstraction barriers for the pro-*R* C1-H-abstraction. It is seen that the consensus ferryl oxidant Fe^{IV}=O

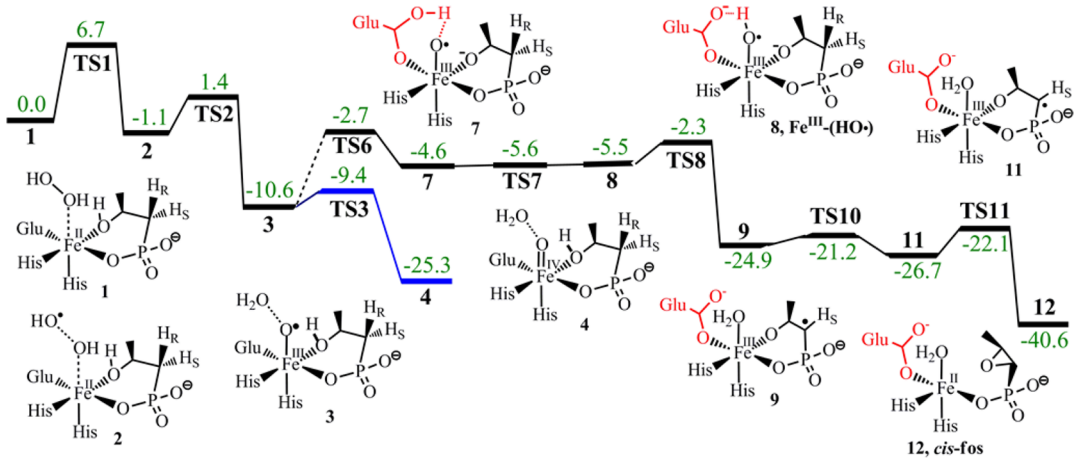

Figure 5. Entire mechanism of *cis*-fos formation (**12**) from $Fe^{II}(H_2O_2)$, **1** (from Snap-1). Shown are only the lowest-energy steps. The overall rate-determining barrier for this process is 23.0 kcal/mol (from the ferryl **4** to **TS8**).

DOI: 10.1021/jacs.6b03555
J. Am. Chem. Soc. 2016, 138, 8489–8496

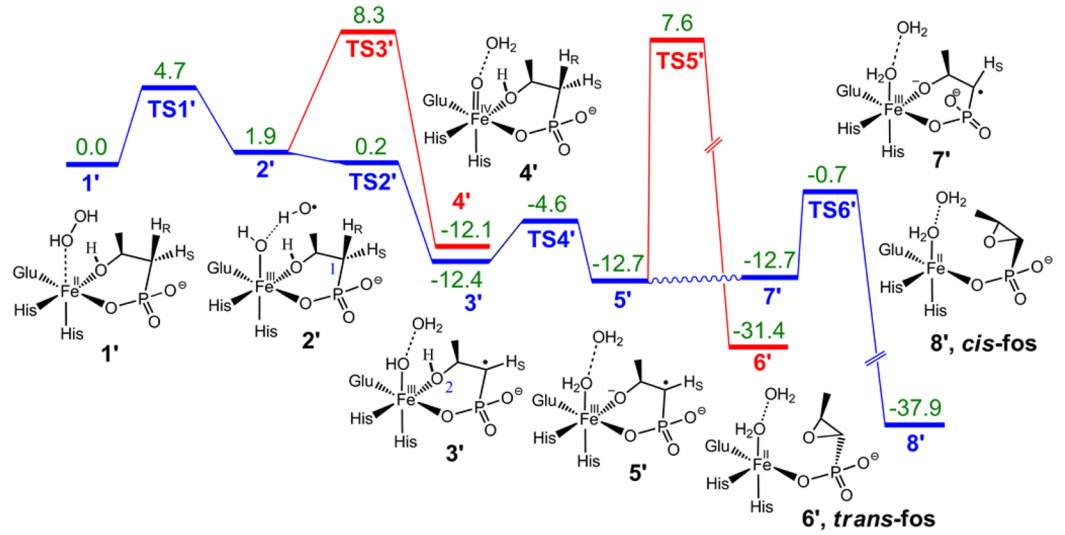

Figure 6. Entire mechanism of *cis*-fos formation (**8′**) from $Fe^{II}(H_2O_2)$ **1′** (from Snap-2). The lowest-energy mechanism is traced in a blue color, while the paths not taken are in red color. The rate-determining barrier is 12.0 kcalmol, referring to the transformation of **7′** to **8′** via **TS6′**. Note the labels in two mechanisms (Snap-1 and -2) do not always match as the two mechanisms involve different species.

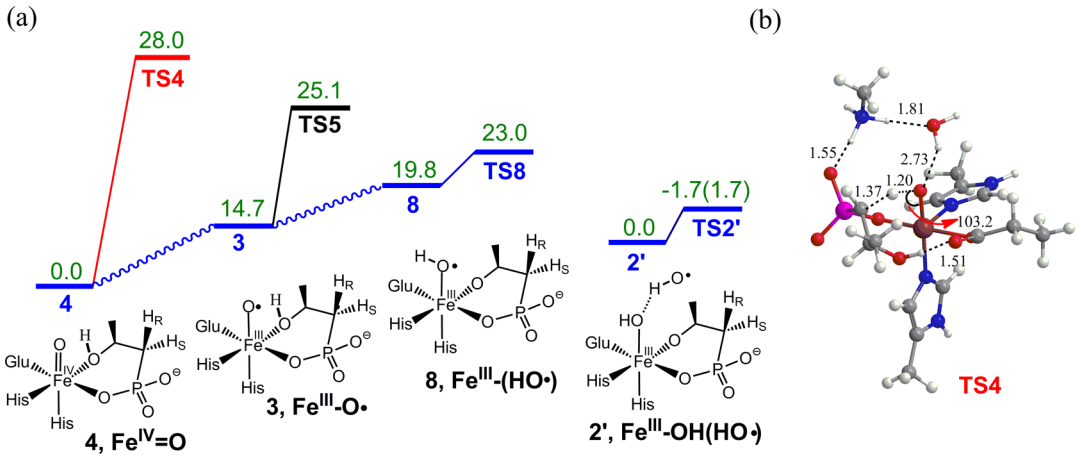

Figure 7. (a) Using the QM/MM (UB3LYP/B2) barriers of the pro-*R* C1-H-abstraction to rank the oxidation capabilities of Fe^{IV}═O, Fe^{III}–O•, Fe^{III}–(HO•), and Fe^{III}–OH(HO•) species. Note that for **TS2′**, the inclusion of ZPE and dispersion corrections leads to a negative barrier, while the corresponding UB3LYP/B2 barrier without any corrections is positive and shown in parentheses. (b) QM/MM (UB3LYP/B1) optimized structures (in Å) of the H-abstraction TS of the ferryl species, **TS4**.

has the highest barrier, while the oxyl Fe^{III}–O• has the second highest. These are the poorest oxidants. As we mentioned above, due to orbital-selection rules, the Fe^{IV}═O oxidant has a clear preference to an Fe–O—H trajectory of ∼180°,[36,38] whereas the intramolecular H-abstraction by Fe^{IV}═O is constrained to ∼103° (Figure 7b) thus leading to a high barrier.[37] The oxyl species has a similar requirement, and hence it is not a great oxidant. On the other hand, the coordinated hydroxyl radicals, Fe^{III}–(HO•) and Fe^{III}–OH(HO•), are flexible and, as such, are by far the better oxidants. Both oxidants are equipped with an HO• radical, which is not strongly bound and is capable of assuming the correct trajectory for H-abstraction, leading to a tiny barrier for H-abstraction. It is clear that neither Fe^{IV}═O nor its electromer Fe^{III}–O• is competitive with the coordinated hydroxyl radicals in driving this crucial step of intramolecular H-abstraction that leads to the observed product. This is why HppE evolved to use these oxidants.

It is intriguing how enzymes manage to violate any preconceived consensus! Thus, whereas the Fe^{IV}═O species is considered to be the primary reactive intermediate in the catalytic cycles of numerous nonheme iron enzymes and synthetic complexes, the present findings show that HppE violates the consensus[39,40] and generates a loosely bonded HO• radical to carry out the energy-demanding H-abstraction reaction.

4. CONCLUSION

This study may have far-reaching implications on the C–H activation reactions in chemistry and biochemistry. Our computations show that upon homolysis of Fe^{II}(HO–OH), or the protonation of the Fe^{IV}═O species, HppE generates highly reactive species, Fe^{III}–OH(HO•) and Fe^{III}–(HO•), which function herein as an important oxidants in selective C–H activation. Indeed, the hydroxyl radical (HO•) is one of the most powerful and prevalent oxidants,[41] which has been shown commonly to react unselectively with the surrounding protein

DOI: 10.1021/jacs.6b03555
J. Am. Chem. Soc. 2016, 138, 8489–8496

and thus destroying the enzymatic activity. However, in HppE, the weak binding of HO• by the Fe^{III}−OH and Fe(III) centers and the coordination of the HO• radical by H-bonding to the protein generate new oxidants, which are highly reactive and selective to the *cis*-fos product. It is important to recognize that the action of HO• radical found here for HppE is not some artifact. It is the way nonheme enzymes found to carry out a difficult H abstraction, for which the consensus Fe^{IV}=O oxidant requires a trajectory of ∼180° for the Fe−O−H angle, which cannot be met in the intramolecular H-abstraction.[36−38] Thus, other nonheme iron enzymes and synthetic complexes may use the same powerful oxidants.

Finally, our findings may also have implications on the Fenton chemistry, which is common process in vivo and in vitro. The Fenton reaction (eq 1) can produce the HO• radical.[7] Starting from the product of eq 1, two competing pathways can be envisaged. One is the homolysis of the O−O bond and formation of the radical Fe^{III}−OH (HO•) species (eq 2a), which can get free in the absence of proper H-bonding.

$$Fe^{II} + H_2O_2 \rightarrow Fe^{III} + OH^- + HO^\bullet \quad (1)$$

$$Fe^{II} + H_2O_2 \rightarrow Fe^{III}{-}OH(HO^\bullet) \quad (2a)$$

$$Fe^{II} + H_2O_2 \rightarrow Fe^{III}{-}OH(HO^\bullet) \quad (2b)$$

$$Fe^{II} + H_2O_2 \rightarrow Fe^{III}{-}(HO^\bullet) + OH^- \quad (3)$$

The other pathway is eq 3, where the binding of the HO• radical leads to formation of an Fe^{III}−(HO•) intermediate. Either Fe^{III}−OH (HO•) and/or Fe^{III}−(HO•) can serve as potent and selective oxidants. The formation of Fe^{III}−(HO•) was postulated by Imlay long ago in the biological Fenton system,[42] and its first such demonstration may be our computational study. Thus, our study shows that Fe^{III}−(HO•) and/or Fe^{III}−OH (HO•) can be formed in the biological Fenton system, which could be highly reactive species that nevertheless perform selective C−H activation. Fe^{III}−(HO•) is formed in an interesting manner by intramolecular proton transfer from the basal ligand to Fe=O (Figure 5). This powerful oxidant can be designed in mimetic systems by using appropriate ligands.

As such, the present work expands the landscape of nonheme iron enzymes and links these enzymes to Fenton chemistry, in a manner that may hopefully guide experiments to design the new biocatalysts and synthetic catalysts that can perform challenging C−H bond functionalizations that cannot accommodate the orbital selection rules of the consensus active species.[36,37]

■ ASSOCIATED CONTENT

Supporting Information

The Supporting Information is available free of charge on the ACS Publications website at DOI: 10.1021/jacs.6b03555.

Total QM/MM energies, zero-point energies (ZPE), as well as Cartesian coordinates of all computed species (PDF)

■ AUTHOR INFORMATION

Corresponding Authors

*binju.wang@gmail.com
*wenzhenlai@ruc.edu.cn
*sason@yfaat.ch.huji.ac.il

Notes

The authors declare no competing financial interest.

■ ACKNOWLEDGMENTS

The work is supported by an Israel Science Foundation grant (ISF-1183/13) to S.S. B.W. and K.D.D. acknowledge the Planning and Budgeting Committee (PBC) of the council for higher education in Israel for the Post Doctoral Fellowships. W.Z.L. is supported by the National Natural Science Foundation of China (no. 21203245).

■ REFERENCES

(1) Groves, J. T. *J. Inorg. Biochem.* **2006**, *100*, 434−447.
(2) (a) Krebs, C.; Fujimori, D. G.; Walsh, C. T.; Bollinger, J. M., Jr. *Acc. Chem. Res.* **2007**, *40*, 484−492. (b) Nam, W. *Acc. Chem. Res.* **2007**, *40*, 522−531. (c) Que, L., Jr. *Acc. Chem. Res.* **2007**, *40*, 493−500.
(3) (a) Blomberg, M. R. A.; Borowski, T.; Himo, F.; Liao, R.-Z.; Siegbahn, P. E. M. *Chem. Rev.* **2014**, *114*, 3601−3658. (b) Kamachi, T.; Yoshizawa, K. *J. Am. Chem. Soc.* **2003**, *125*, 4652−4661.
(4) Zheng, G.; Fu, Y.; He, C. *Chem. Rev.* **2014**, *114*, 4602−4620.
(5) Chang, W. C.; Guo, Y.; Wang, C.; Butch, S. E.; Rosenzweig, A. C.; Boal, A. K.; Krebs, C.; Bollinger, J. M., Jr. *Science* **2014**, *343*, 1140−1144.
(6) Wong, S. D.; Srnec, M.; Matthews, M. L.; Liu, L. V.; Kwak, Y.; Park, K.; Bell, C. B., III; Alp, E. E.; Zhao, J. Y.; Yoda, Y.; Kitao, S.; Seto, M.; Krebs, C.; Bollinger, J. M.; Solomon, E. I. *Nature* **2013**, *499*, 320−323.
(7) Fenton, H. J. H. *J. Chem. Soc., Trans.* **1894**, *65*, 899−910.
(8) Poulos, T. L. *Chem. Rev.* **2014**, *114*, 3919−3962.
(9) Liu, P. H.; Liu, A. M.; Yan, F.; Wolfe, M. D.; Lipscomb, J. D.; Liu, H. W. *Biochemistry* **2003**, *42*, 11577−11586.
(10) Liu, P. H.; Murakami, K.; Seki, T.; He, X. M.; Yeung, S. M.; Kuzuyama, T.; Seto, H.; Liu, H. W. *J. Am. Chem. Soc.* **2001**, *123*, 4619−4620.
(11) Liu, P. H.; Mehn, M. P.; Yan, F.; Zhao, Z. B.; Que, L.; Liu, H. W. *J. Am. Chem. Soc.* **2004**, *126*, 10306−10312.
(12) Higgins, L. J.; Yan, F.; Liu, P. H.; Liu, H. W.; Drennan, C. L. *Nature* **2005**, *437*, 838−844.
(13) Wang, C.; Chang, W. C.; Guo, Y. S.; Huang, H.; Peck, S. C.; Pandelia, M. E.; Lin, G. M.; Liu, H. W.; Krebs, C.; Bollinger, J. M. *Science* **2013**, *342*, 991−995.
(14) Huang, H.; Chang, W. C.; Lin, G. M.; Romo, A.; Pai, P. J.; Russell, W. K.; Russell, D. H.; Liu, H. W. *J. Am. Chem. Soc.* **2014**, *136*, 2944−2947.
(15) Chang, W. C.; Dey, M.; Liu, P. H.; Mansoorabadi, S. O.; Moon, S. J.; Zhao, Z. B. K.; Drennan, C. L.; Liu, H. W. *Nature* **2013**, *496*, 114−118.
(16) Nam, W.; Lee, Y.-M.; Fukuzumi, S. *Acc. Chem. Res.* **2014**, *47*, 1146−1154.
(17) Puri, M.; Que, L., Jr. *Acc. Chem. Res.* **2015**, *48*, 2443−2452.
(18) Milaczewska, A.; Broclawik, E.; Borowski, T. *Chem. - Eur. J.* **2013**, *19*, 771−781.
(19) Warshel, A. *Angew. Chem., Int. Ed.* **2014**, *53*, 10020−10031.
(20) Senn, H. M.; Thiel, W. *Angew. Chem., Int. Ed.* **2009**, *48*, 1198−1229.
(21) Lin, H.; Truhlar, D. G. *Theor. Chem. Acc.* **2007**, *117*, 185−199.
(22) (a) van der Kamp, M. W.; Mulholland, A. J. *Biochemistry* **2013**, *52*, 2708−2728. (b) Harvey, J. N.; Bathelt, C. M.; Mulholland, A. J. *J. Comput. Chem.* **2006**, *27*, 1352−1362.
(23) Olsson, M. H.; Søndergard, C. R.; Rostkowski, M.; Jensen, J. H. *J. Chem. Theory Comput.* **2011**, *7*, 525−537.
(24) Brooks, B. R.; Brooks, C. L.; III; MacKerell, A. D., Jr.; Nilsson, L.; Petrella, R. J.; Roux, B.; Won, Y.; Archontis, G.; Bartels, C.; Boresch, S.; Caflisch, A.; Caves, L.; Cui, Q.; Dinner, A. R.; Feig, M.; Fischer, S.; Gao, J.; Hodoscek, M.; Im, W.; Kuczera, K.; Lazaridis, T.; Ma, J.; Ovchinnikov, V.; Paci, E.; Pastor, R. W.; Post, C. B.; Pu, J. Z.; Schaefer, M.; Tidor, B.; Venable, R. M.; Woodcock, H. L.; Wu, X.;

DOI: 10.1021/jacs.6b03555
J. Am. Chem. Soc. 2016, 138, 8489−8496

Yang, W.; York, D. M.; Karplus, M. *J. Comput. Chem.* **2009**, *30*, 1545−1614.
(25) (a) Sherwood, P.; de Vries, A. H.; Guest, M. F.; Schreckenbach, G.; Catlow, C. R. A.; French, S. A.; Sokol, A. A.; Bromley, S. T.; Thiel, W.; Turner, A. J.; Billeter, S.; Terstegen, F.; Thiel, S.; Kendrick, J.; Rogers, S. C.; Casci, J.; Watson, M.; King, F.; Karlsen, E.; Sjovoll, M.; Fahmi, A.; Schäfer, A.; Lennartz, C. *J. Mol. Struct.: THEOCHEM* **2003**, *632*, 1−28. (b) Metz, S.; Kästner, J.; Sokol, A.; Keal, T.; Sherwood, P. *WIREs Comput. Mol. Sci.* **2014**, *4*, 101−110.
(26) Ahlrichs, R.; Bär, M.; Häser, M.; Horn, H.; Kölmel, C. *Chem. Phys. Lett.* **1989**, *162*, 165−169.
(27) Smith, W.; Forester, T. R. *J. Mol. Graphics* **1996**, *14*, 136−141.
(28) Bakowies, D.; Thiel, W. *J. Phys. Chem.* **1996**, *100*, 10580−10594.
(29) Becke, A. D. *J. Chem. Phys.* **1993**, *98*, 5648−5652.
(30) Billeter, S. R.; Turner, A. J.; Thiel, W. *Phys. Chem. Chem. Phys.* **2000**, *2*, 2177−2186.
(31) Grimme, S.; Antony, J.; Ehrlich, S.; Krieg, H. *J. Chem. Phys.* **2010**, *132*, 154104−154109.
(32) Kumar, D.; Thiel, W.; de Visser, S. P. *J. Am. Chem. Soc.* **2011**, *133*, 3869−3882.
(33) Schyman, P.; Lai, W. Z.; Chen, H.; Wang, Y.; Shaik, S. *J. Am. Chem. Soc.* **2011**, *133*, 7977−7984.
(34) Wang, B.; Usharani, D.; Li, C.; Shaik, S. *J. Am. Chem. Soc.* **2014**, *136*, 13895−13901.
(35) Wang, B.; Li, C.; Dubey, K. D.; Shaik, S. *J. Am. Chem. Soc.* **2015**, *137*, 7379−7390.
(36) Usharani, D.; Janardanan, D.; Li, C.; Shaik, S. *Acc. Chem. Res.* **2013**, *46*, 471−482.
(37) Mas-Ballesté, R.; McDonald, A. R.; Reed, D.; Usharani, D.; Schyman, P.; Milko, P.; Shaik, S.; Que, L., Jr. *Chem. - Eur. J.* **2012**, *18*, 11747−11760.
(38) Shaik, S.; Chen, H.; Janardanan, D. *Nat. Chem.* **2011**, *3*, 19−27.
(39) Another nonconsensual nonheme oxidant was recently proposed in: Wang, Y.; Janardanan, D.; Usharani, D.; Han, K.; Que, L., Jr.; Shaik, S. *ACS Catal.* **2013**, *3*, 1334−1341.
(40) For isolation and reactivity of the oxidant in ref 39, see: Serrano-Plana, J.; Oloo, W. N.; Acosta-Rueda, L.; Meier, K. K.; Verdejo, B.; Garcia-Espana, E.; Basallote, M. G.; Munck, E.; Que, L., Jr.; Company, A.; Costas, M. *J. Am. Chem. Soc.* **2015**, *137*, 15833−15842.
(41) Gligorovski, S.; Strekowski, R.; Barbati, S.; Vione, D. *Chem. Rev.* **2015**, *115*, 13051−13092.
(42) Imlay, J. A.; Chin, S. M.; Linn, S. *Science* **1988**, *240*, 640−642.

DOI: 10.1021/jacs.6b03555
J. Am. Chem. Soc. 2016, 138, 8489−8496